6
Integral Sliding mode Control for PFC and ZSC Converters

Sliding mode control, discussed in previous Chapters, makes the system invariant to external disturbances once the system trajectories reach the designed sliding surface. However, it takes finite time to reach the surface from the initial point, known as the reaching phase. During this reaching phase the system is susceptible to noise. This Chapter discusses Integral Sliding Mode Control (ISMC) which eliminates the reaching phase and hence makes the system robust from the starting point. Moreover it combines with the existing classical linear control methods which have also been applied and researched for the power factor correction. The dual-loop PID control is one of the conventional classical control methods for mitigating the harmonics in input current in PFC converters. It owes its widespread acceptance due to the ease of design process and established frequency domain control theory for linear control. These classical controls perform well at the operating point, however, these control compromise among the dynamic performance, robustness and stability at the large line-load transients. Moreover, the actual power converters are subjected to disturbances or uncertainty in the system such as parametric variations, exogenous disturbances, sensor's noise and disturbances caused by magnetic components, unmodeled system dynamics. Thus, non-linear control approaches are better choice in the systems having frequent large line-load transients and uncertainty in the system parameters.

Hence, from the user point of view, a linear control is preferred for ease of design while using non-linear control gives system robustness. Therefore, there is a need of control techniques which combine the merits of the classical control and modern non-linear control. The concept of integral sliding mode (ISM) control discussed in this work, provides solution to take benefits of classical control technique and sliding mode control.

The integral sliding mode (ISM) control is one of the non-linear robust control approaches [Loukianov *et al.*, 2006], [Rubagotti *et al.*, 2011]. Many researches have proposed integral sliding surfaces, however, ISM control is substantially different than these surfaces. In ISM control, the dynamic performance is guaranteed by nominal controller and ISM controller rejects only disturbances.The nominal controller can be designed by any methodology i.e. PI, optimal, H_∞; the ISM control methodology adds a non-linear controller to the nominal controller and thus overall control law is obtained. The combined control is robust and possesses invariance property against the matched uncertainty [Utkin and Shi, 1996]. Furthermore, the nominal classical control such as conventional dual-loop control method mitigates harmonics in the input current for the nominal and normal operating conditions only. In the conditions like that of parametric variations, the desired power factor may not be achieved. The ISM based control approach allows leveraging benefits of both, linear and non-linear control, by employing a combination of continuous nominal controller (for stabilizing the nominal system without any disturbances) and a discontinuous sliding mode controller to compensate for perturbations occurring in the system. Additionally, it also addresses the reaching phase issue related to conventional SMC by including an integral term while designing the sliding surface. This ensures that the ISMC eliminates the reaching phase, thus guaranteeing robustness from the initial instant.

In this work, a dual loop PI-controller (nominal controller) amalgamates with ISM con-

troller. The proposed ISM based controller is used for power factor correction. In the literature, to the best of author's knowledge, the application of the classical control in conjunction with the ISM based control is not addressed for the power factor correction in particular. This is the motivation behind the work. Moreover, it is also able to compensate for the reduced size inductance and capacitance. This aspect of ISM, of being able to maintain the system performance even under system parameter variation, motivated the a parametric analysis work on Z-source converters.

Z-source converter is usually modelled as a fifth order system with two capacitors voltages and two inductor current of the Z-network along with the load current as state variables. However, based on the symmetry of the Z-source the system model is reduced to third order for the ease of analysis and reduced complexities in controller design. Nonetheless, this symmetry in the Z-source network is an ideal case because duplicating two elements is infeasible. Therefore, the system dynamics cannot be represented by the reduced order model and a controller designed using the reduced order model can no longer suffice. The proposed non-linear ISM controller mitigates this uncertainty in parameters if they lie in the matched space (input subspace) of the system.

This Chapter presents an integral sliding mode based controller amalgamated with dual loop PI-controller (nominal controller) for the PFC applications. The proposed controller makes the system robust from the initial point against external disturbances and system parametric variation. The work is then explored to study Z-source converters with parametric uncertainties. The Chapter is organized as follows. The principle of ISMC is discussed in Section 6.1. This section also included the choice of switching surface, control law and the proof for the existence of sliding mode. In Section 6.2 ISMC application for PFC application is presented. This section included the system description, design of nominal and ISM control followed by simulation studies for the boost PFC. In Section 6.3, the proposed ISM based controller is proposed for Z-source converter. This section included system description, design of nominal and ISM control, effect of asymmetry on system performance of ZSC, followed by relevant simulation results. Section 6.4 summarizes the Chapter.

6.1 PRINCIPLE OF ISM BASED CONTROLLER

This section discusses the basic methodology of the ISM controller. It demonstrates the effectiveness of the controller to eliminate the matched disturbances. Moreover, the choice of switching surface for stable sliding mode, control law to make the trajectories move towards the switching surface and, the existence of the sliding motion using the chosen switching surface and control law has been presented here, for a generic system. It also presents the procedure to separate the matched and unmatched disturbances for a practical system. The author would like to state here that the concept of ISM based control and the analysis has been carried out in light of the work covered in [Rubagotti *et al.*, 2011], [Castaños and Fridman, 2006].

The important feature of ISM control is, it allows SMC to combine with a nominal control e.g. classical control such as PID control, LQR [Utkin and Shi, 1996], [Bandyopadhyay *et al.*, 2009]. The system dynamics are governed by nominal control. However, nominal control, generally, does not eliminate the uncertainty/disturbances in the system. The ISM based control, which is added to the nominal control, eliminates the matched uncertainty/disturbances from the very beginning of system response [Rubagotti *et al.*, 2011]. Therefore, the overall performance of the system improves.

To understand the principle of ISMC, consider a dynamic model of a system with uncertainty as,

$$\dot{x} = f(x) + g(x)u + \psi \tag{6.1}$$

Here, ψ is a matched disturbance, i.e. it lies in the subspace of input such that $\psi = B\psi_m$. From a

control point of view, the matching condition means that the effects produced by ψ_m in the system can be produced by u, and vice versa. Moreover, the upper bound of the uncertainty ψ_m is known, let that be λ.
The ideal system dynamics i.e. when system is operating using nominal control u_o, without any disturbance, is given as

$$\dot{x_o} = f(x_o) + g(x_o)u_o \tag{6.2}$$

The aim is to choose u in (6.1) of the form $u = u_o + u_n$ such that it compensates for the uncertainty in the system and system trajectories follow $x(t) = x_o(t)$ at all times.

The design process involves choosing a sliding surface that ensures sliding mode from the very beginning of the system response. The integral switching function can be chosen as [Utkin and Shi, 1996], [Castaños and Fridman, 2006].

$$s(x,t) = G[x(t) - x(0) - \int_0^\tau \{f(x(\tau)) + g(x(\tau))u_o(x(\tau))\}d\tau] \tag{6.3}$$

Here, $G \in \mathbb{R}^{mxn}$ is a full rank matrix to be designed such that $det(Gg(x)) \neq 0$. u_o is the nominal control and in contrast with conventional sliding modes, here an integral term is included.

The control signal ensuring the existence of sliding mode can be obtained by equating $\dot{s} = 0$. Solving this for u gives equivalent control as follow,

$$\dot{s} = Gg(x)(u_n + \psi_m) \tag{6.4}$$

Thus, $u_{neq} = -\psi_m$ and one of the choices of u_n is

$$u_n = -\eta(Gg(x))^{-1} sign(s) \tag{6.5}$$

In order to enforce the sliding motion value of η is kept slightly higher than the maximum disturbance i.e. $\eta > \lambda$.

6.1.1 Switching Surface

The stability of the sliding mode depends on the choice of the switching surface, therefore the important task is to choose an integral switching matrix G that ensures sliding mode from the very beginning of the system response. The integral switching function can be chosen as [Utkin and Shi, 1996], [Castaños and Fridman, 2006].

$$s(x,t) = G[x(t) - x(0) - \int_0^\tau \{f(x(\tau)) + g(x(\tau))u_o(x(\tau))\}d\tau] \tag{6.6}$$

The term $x(0) + \int_0^\tau \{f(x(\tau)) + g(x(\tau))u_o(x(\tau)\}d\tau$ can be thought of as a trajectory of the system, obtained by the nominal control $u_o(x,t)$, in the absence of perturbation term $\psi_m(x,t)$. In (6.6), at $t = 0$, $s(x,0) = 0$. Hence, from the initial time instance, the system states are at sliding surface, this implies that the reaching-phase is eliminated.

6.1.2 Control Law

The next step in the design of ISM is to design a control law which guarantees that the system trajectories reach the designed switching surface in finite time. The control, typically consists of two parts; a linear part and a non-linear part such that

$$u = u_o + u_n \tag{6.7}$$

Here, u_n is the non-linear part with a discontinuous component and is responsible for bringing about sliding motion on s. The nominal control input u_o is responsible for helping to maintain sliding. One of the choices of u_n is

$$u_n = -\eta(Gg(x))^{-1} sign(s) \tag{6.8}$$

Here, η is a scalar gain chosen to be larger than the maximum bound of the uncertainty present in the system, in order to enforce the sliding motion i.e. $\eta > \lambda$.

6.1.3 Existence of Sliding mode

The choice of the integral switching function given by (6.6) ensures that the sliding mode begins at t = 0. Mathematically, a strong reachability condition, which ensures finite reaching of the trajectories even under disturbances, is given by (6.9). This is called η-reachability condition and is analysed here.

$$s(x,t).\dot{s}(x,t) = -\eta|s(x,t)| \tag{6.9}$$

To prove existence, let the Lyapunov function as,

$$V = \frac{s(x,t)^2}{2} \tag{6.10}$$

Then the time-derivative of V gives,

$$\dot{V} = s(x,t).\dot{s}(x,t) \tag{6.11}$$

Now, from the derivative of (6.6) we get,

$$\dot{s}(x,t) = G\dot{x}(t) - G\{f(x(t)) + g(x(t))u_o\} \tag{6.12}$$

Using (6.12) in (6.11),

$$\dot{V} = s(x,t)[G\dot{x}(t) - G\{f(x(t)) + g(x(t))u_o\}] \tag{6.13}$$

Using any generic system $\dot{x} = f(x(t)) + g(x(t))u$, in (6.13)

$$\dot{V} = s(x,t))\{Gg(x(t))(u - u_o)\} \tag{6.14}$$

Substituting (6.7) in (6.14)

$$\dot{V} = s(x,t)\{Gg(x(t))u_n\} \tag{6.15}$$

One of the choices of discontinuous control u_n in (6.7) is $u_n = -\eta(Gg(x(t)))^{-1} sign(s)$

$$\dot{V} = -\eta s(x,t) sign(s(x,t)) \tag{6.16}$$

$$\dot{V} = -\eta|(s(x,t))| \tag{6.17}$$

Here, $|s(x,t)| = s(x,t)sign(s(x,t))$. To satisfy $\dot{V} < 0$, in (6.17), η must be a positive number. Hence, by design $\eta > 0$. This ensures $\eta-$reachability condition. In the design of ISM control, it is sufficient to choose control parameter G such that the inverse of $Gg(x(t))$ exists. However, an optimal choice of G given by (6.18) ensures that the unmatched disturbances do not amplify.

$$G = g^+(x(t)) = \{g^T(x(t))g(x(t))\}^{-1} g^T(x(t)) \tag{6.18}$$

A common choice of discontinuous control u_n is,

$$u_n = -\eta(Gg(x(t)))^{-1} \frac{s}{||s||} \tag{6.19}$$

If the system under consideration has single input, (6.19) reduces to,

$$u_n = -\eta(Gg(x(t)))^{-1} sign(s) \tag{6.20}$$

Here, $sign(s) = \frac{s}{||s||}$. Suppose the maximum upper bound of the ψ_m is $\lambda = ||\psi_m||$, then by design $\eta > \lambda$.

6.2 SINGLE STAGE BOOST PFC APPLICATION

This section presents the proposed ISM control for the Boost PFC application. From small signal model of the Boost system to the design of the nominal dual-loop PI control and proposed ISM control, a detailed analysis is covered here. Results highlighting the effectiveness of the proposed controller is also demonstrated in the Section.

6.2.1 System Description and dynamic model

A circuit of the non-isolated boost power factor correction converter is shown in Fig. 6.1. The bridge rectifier is fed by a sinusoidal AC voltage. At the output of which, a boost converter is

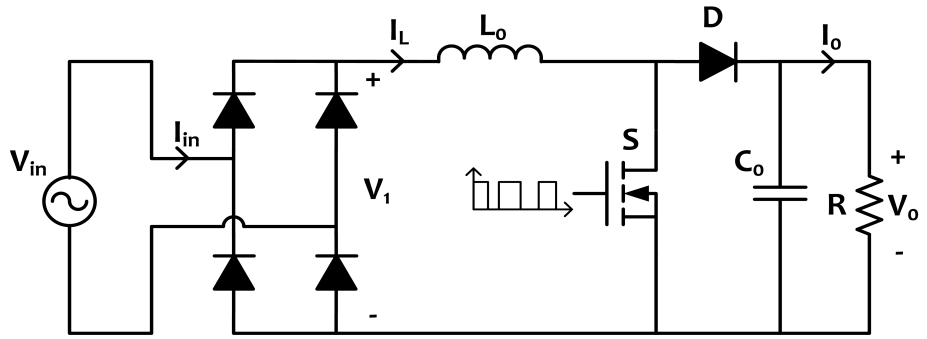

Figure 6.1 : PFC based on a boost converter

connected. The converter dynamics can be represented mathematically using state-space averaging as:

$$\dot{x_1} = \frac{-x_2}{L_o}(1-u)+\frac{v_1}{L_o} \tag{6.21a}$$

$$\dot{x_2} = \frac{x_1}{C_o}(1-u)+\frac{-x_2}{RC_o} \tag{6.21b}$$

Where, x_1 and x_2 are the states of the system representing Inductor Current and Output Voltage respectively. u is the control input. v_1 is the rectified input voltage and L_o, C_o, and R are the inductance, capacitance and load resistance respectively.

This is to mention that for this application widely adopted dual-loop PID controller is chosen as the nominal control. To design a linear controller, a linear dynamic model is required, which is developed using small-signal perpetuation method. The variables after perturbation are given as $x_1 = x_{1r}+\tilde{x_1}; x_2 = x_{2r}+\tilde{x_2}; E = E_o+\tilde{E}; u = D_0+d$. Here ($\tilde{}$) represents the small-signal value. d is the perturbed part of the input control signal. $x_{1r}; x_{2r}; D_0; E_o$ are the nominal operating conditions. The small signal model, presented in (6.22), is obtained using perturbed variables in (6.21) and collecting only AC terms.

$$\begin{bmatrix}\dot{\tilde{x_1}}\\ \dot{\tilde{x_2}}\end{bmatrix} = \begin{bmatrix}0 & -\frac{1}{L_o}\\ \frac{1}{C_o} & -\frac{1}{RC_o}\end{bmatrix}\begin{bmatrix}\tilde{x_1}\\ \tilde{x_2}\end{bmatrix} + \begin{bmatrix}\frac{x_{2r}}{L_o}\\ -\frac{x_{1r}}{C_o}\end{bmatrix} d + \begin{bmatrix}\frac{\tilde{E}}{L_o}\\ 0\end{bmatrix} \tag{6.22}$$

The transfer function obtained using Laplace-transform of (6.22) in order to design the nominal controller are given below.

- The Control input to output voltage transfer function

$$T_{vd}(s) = \left.\frac{\tilde{x_2}(s)}{d(s)}\right|_{\tilde{E}(s)=0} = \frac{x_{2r}(1-D_o)-sx_{1r}L_o}{s^2L_oC_o+s\frac{L_o}{R}+(1-D_o)^2} \tag{6.23}$$

- The Control input to inductor current transfer function

$$T_{id}(s) = \frac{\tilde{x_1}(s)}{d(s)}\bigg|_{\tilde{E}(s)=0} = \frac{sC_0x_{2r} + 2(1-D_o)x_{1r}}{s^2L_oC_o + s\frac{L_o}{R} + (1-D_o)^2} \tag{6.24}$$

- The inductor current to output voltage transfer function

$$T_{vi}(s) = \frac{\tilde{x_2}(s)}{\tilde{x_1}(s)}\bigg|_{\tilde{E}(s)=0,d(s)=0} = \frac{x_{2r}(1-D_o) - sx_{1r}L_o}{sC_0x_{2r} + 2(1-D_o)x_{1r}} \tag{6.25}$$

6.2.2 Proposed ISM Control (The overall control)

The proposed control ($u = u_o + u_n$) amalgamates a dual-loop PID-control as a nominal controller (u_o) and the sliding mode control as non-linear control (u_n). The PID-control is affected by various parametric variations, unmodeled system dynamics, external disturbances, and sensor's noise. These factors may perturb the actual operating points and may cause unwanted changes in system states. A large variation in the system parameters may lead to instability in the system. Moreover, since a boost converter is a bilinear system, the linearisation of such system dynamics neglects the non-linear terms. Moreover, such disturbances may affect the nominal control input. Therefore, an nominal PID control is designed along with an ISM based controller to eliminate the matched uncertainty/disturbances.

Designing the nominal dual-loop control

PI controllers are widely used for Boost converters, its a linear control approach which requires a good knowledge of the system and precise tuning in order to obtain the desired performances. Indeed, the presence of a right hand plane Zeros (RHPZ) behaviour in the closed loop system makes its control with a single voltage loop more difficult and unsuitable in some cases. A dual loop PI controller was designed for the model given in (6.22). The control structure adopted for the dual loop is given as Fig 6.2. Since capacitor voltage dynamics is slower than the inductor current dynamics, the current loop is chosen as the inner-loop and voltage loop is chosen the outer-loop. Also, this is why, the inductor current reference is generated using voltage error.

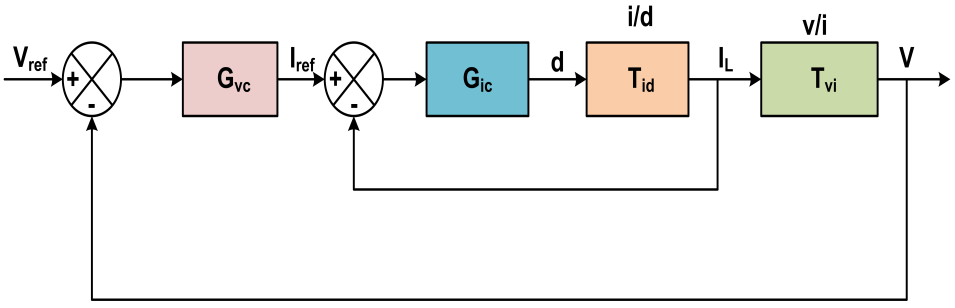

Figure 6.2 : Dual loop control structure

The controller is designed for the converter specification given in Table 6.1.

The control to current output transfer function can be derived from the reduced model as follows

$$T_{id}(s) = \frac{95238(s+30.3)}{(s^2+15.15s+7.792e05)} \tag{6.26}$$

Table 6.1 : System Parameters

Parameter	Value
Boost converter	
Input Voltage Supply	120 V, 50 Hz
Nominal Output voltage	200 V
Inductance (L_o)	2.1 mH
Output capacitor (C_o)	220 μF
Nominal Load R	300 Ω

The PI controller is designed as:

$$G_{ic} = \frac{5s + 0.01}{s} \tag{6.27}$$

The current loop gain can be expressed as

$$G_i = T_{id} G_{ic} \tag{6.28}$$

The Frequency response curve of the open loop transfer function (T_{id}) and the closed loop gain (G_i) for the inner current loop is plotted in Fig. 6.3. The open loop bode plots shows a PM = 89.99 at 95.242 k rad/s. Also, it is needed to improve the low-frequency gain to reduce steady-state error, improve the phase-margin for better transient response. Now, for the outer loop, inductor

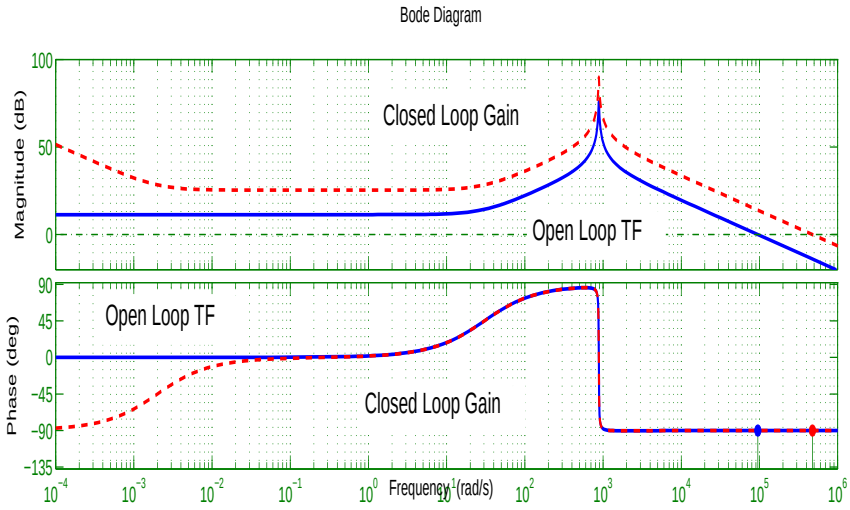

Figure 6.3 : Frequency domain plots for open-loop transfer function and closed-loop gain of the current-loop: (a) magnitude and (b) phase.

current to voltage transfer function is obtained as

$$T_{vi} = \frac{-0.05303(s - 5.143e04)(s^2 + 15.15s + 7.792e05)}{(s + 30.3)(s^2 + 15.15s + 7.792e05)} \tag{6.29}$$

The PI controller adopted is given as

$$G_{vc} = \frac{0.05s+1}{s} \tag{6.30}$$

With the inner current loop closed, the outer voltage loop gain can be expressed as a function of inner current loop gain and associated compensator as

$$G_v = T_{vi}\frac{G_i}{(1+G_i)}G_{vc} \tag{6.31}$$

The Voltage-loop frequency domain plot for open-loop transfer function(T_{vi}) and closed-loop gain (G_v) are shown in Fig. 6.4.

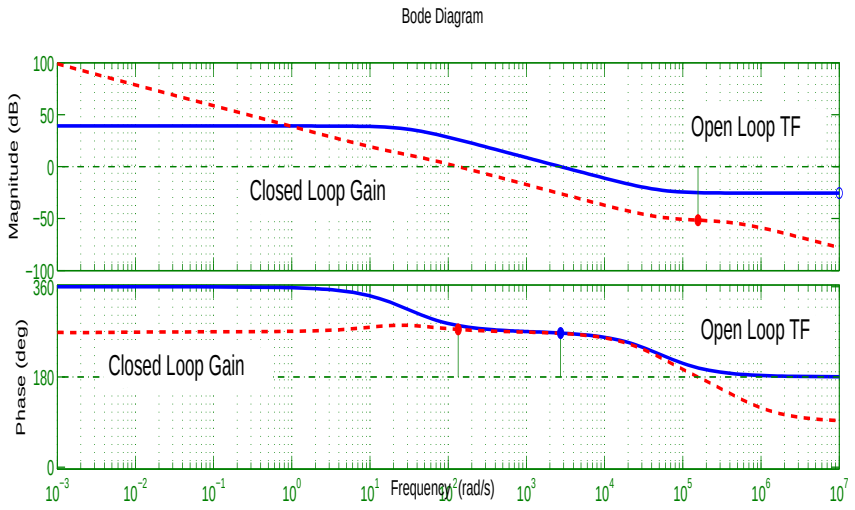

Figure 6.4 : Frequency domain plot for open-loop transfer function and closed-loop gain of the volatge-loop: (a) magnitude and (b) phase.

Design of ISM based Control

Consider a generic dynamic model

$$\dot{x} = f(x(t)) + g(x(t))u$$

this is simplified as follows,

$$\dot{x} = Z\{f_1(x(t)) + g_1(x(t))u\} \tag{6.32}$$

Here, $f_1(x(t)) = Zf(x(t))$ and $g_1(x(t)) = Zg(x(t))$ are function of x and t. Z represents the system parameters matrix. For a boost converter, the system dynamics (6.32) can be written as

$$x(t) := \begin{bmatrix} x_1 \\ x_2 \end{bmatrix}; f_1(x(t)) = \begin{bmatrix} E - x_2 \\ x_1 - x_o \end{bmatrix}; g_1(x(t)) = \begin{bmatrix} x_2 \\ -x_1 \end{bmatrix}; z = \begin{bmatrix} z_1 & 0 \\ 0 & z_2 \end{bmatrix};$$

Here, $z_1 = \frac{1}{L_o}$; $z_2 = \frac{1}{C_o}$.

The switching surface is again

$$s(x,t) = G[x(t) - x(0) - \int_0^\tau \{f(x(\tau)) + g(x(\tau))u_o(x(\tau))\}d\tau] \tag{6.33}$$

Here, the matrix G is chosen as given in (6.34). $x(0)$ is the initial condition. u_0 is the control input of nominal PID controller. The total control input (u) is, $u_o + u_n$. For the present Boost PFC case

$$G = g^{+}(x(t)) = \{g^{T}(x(t))g(x(t))\}^{-1} g^{T}(x(t)) \tag{6.34}$$

$$g(x(t)) := \begin{bmatrix} z_1 x_2 & z_2 x_1 \end{bmatrix}^{T}$$

and

$$g^{+}(x(t)) := \begin{bmatrix} \frac{z_1 x_2}{(z_2 x_1)^2 + (z_1 x_2)^2} & -\frac{z_2 x_1}{(z_2 x_1)^2 + (z_1 x_2)^2} \end{bmatrix}^{T}$$

This implies $Gg(x(t)) = 1$.

The discontinuous control is chosen as

$$u_n = -\eta (Gg(x(t)))^{-1} \frac{s}{||s||} \tag{6.35}$$

The total control is $u = u_o + u_n$. The control is compared against a triangular carrier wave of 25 kHz frequency and generates pulses using pulse width modulation (PWM) method. This pulse train then drives the switch of the Boost PFC converter.

6.2.3 Simulation Studies

In this Section, the results establishing the expediency of the proposed ISM based controller over a nominal controller. It presents comparison between the system response with nominal dual-loop PID controller alone and with proposed ISM based control. These responses are classified into two cases. Case I: Transient response and Case II: Steady state response. The system parameters and nominal operating conditions are kept as given in Table 6.1.

6.2.4 Case I: Transient response

One of the significance of an ISM based control is that it improves system's dynamic response, by making it invariant to matched disturbances, from the initial point. This subsection presents the system response to a load change when controlled using the proposed ISM based strategy.

In Fig. 6.5, the load transient results are shown for the Boost PFC under consideration. The load is varied from 300 Ω to 150 Ω at t = 0.2 sec. At load change, the non-minimum phase nature of the boost converter causes high undershoot. The undershoot in DC-link voltage V_o is < 15 %, however, the voltage settles down at $V_{ref} = 200V$ within 150 ms. It is to be noted the proposed controller maintains high quality of input current through out by maintaining 8.57 % THD at load of 300 Ω is and 9.55 % at 150 Ω.

In Fig. 6.6, the plot of switching function is shown. The switching function is zero from the initial time and remains so for t > 0. Clearly, the proposed ISM controller gives power factor correction along with eliminating matched disturbances and improves line-load transient performance simultaneously unlike the conventional PID based dual-loop control.

6.2.5 Case II: Steady state response

The section, firstly, provides a steady state response to the nominal control at nominal operating conditions, in Fig. 6.7.

As seen the voltage is regulated to its desired value of 200 V and the input current has good quality with a %THD of 9.6 %.

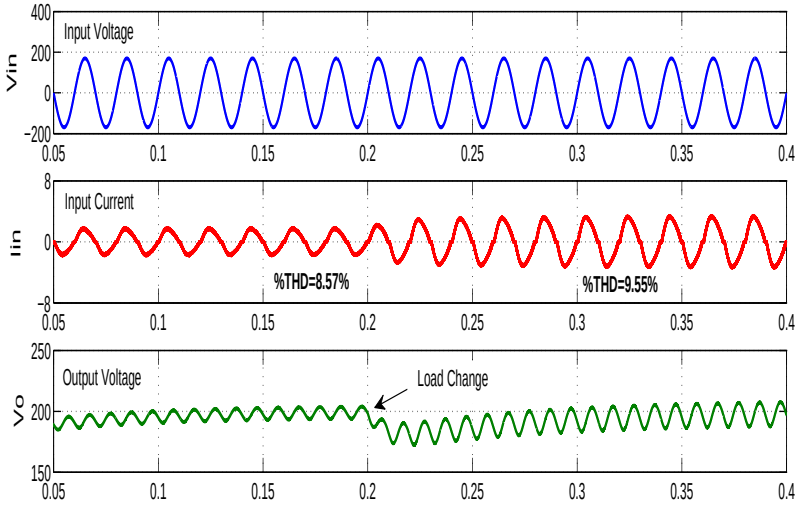

Figure 6.5 : Load transient operation results with proposed ISM based controller

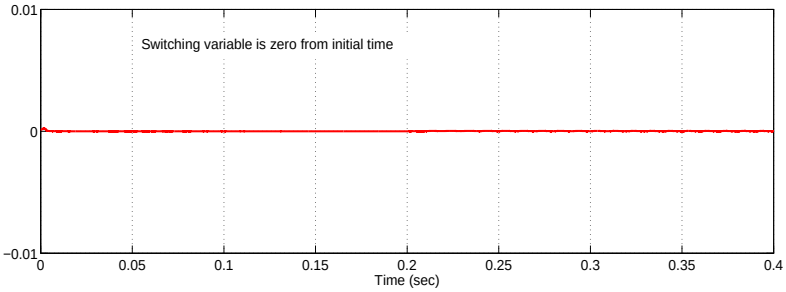

Figure 6.6 : Plot of the switching function s

The Fig. 6.7, is set as the reference for further analysis. Now, the following results present the system responses when perturbation are brought about in the nominal operating conditions. The response corresponding to using nominal PID-controller alone and with ISM based control for the two cases i.e. (a) with external disturbance (b) with reduced size of system parameters, are shown here.

Response to external disturbance

The effect of disturbance entering through the control input with the PID controller alone is shown in Fig. 6.8. A 500 Hz-sinusoidal external disturbance with magnitude 0.2 is added in the control input $\tilde{d} = 0.2sin(2\pi 500t)$, keeping all other conditions to be nominal.

(a) **Performance of Nominal controller against disturbance**

As seen, the PID controller can not compensate for this uncertainty in the input channel and the % THD shoots from nominal 9.6 % (see Fig. 6.7) to 14.75 %.
Now, similar conditions are tested using PID with ISM based control and the corresponding system response is shown in Fig. 6.9. To nullify the effect of external disturbance, the value of η is

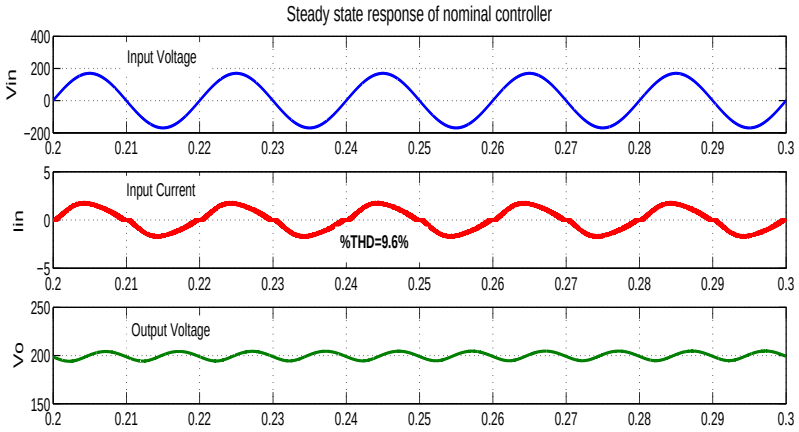

Figure 6.7 : Steady state response using nominal controller.

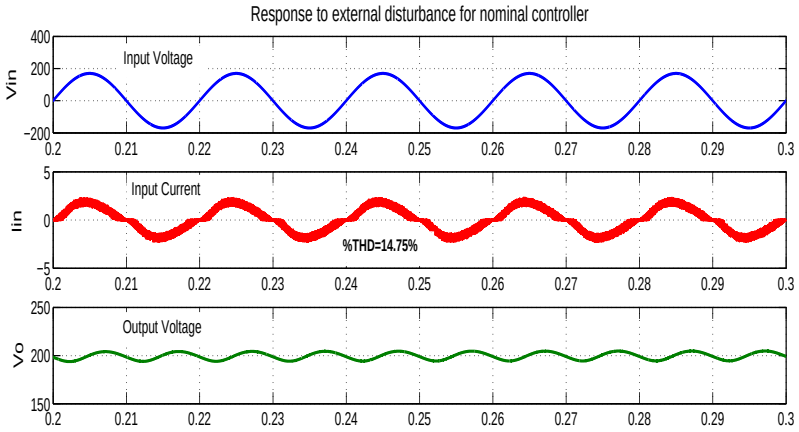

Figure 6.8 : System response using nominal controller against the external disturbance.

kept greater than 0.2 that is higher than the amplitude of sinusoidal disturbance, as required in design.

(b) **Performance of combined Nominal and ISM Controller against disturbance**

The response shows that the proposed ISM based controller can provide compensation for the matched external disturbance and restricts %THD to 8.27 %.

Response to uncertainty in parameters

In this section, the system response to parametric variation is presented. For the test case, system inductance L_o is reduced from 2.1 mH to 1 mH. Effect of parameter reduction with nominal controller as well as with proposed ISM control are shown in Fig. 6.10 and Fig. 6.11, respectively.

Using nominal size of L, C with PID-controller alone, the % THD in input current is 9.6 % (see Fig. 6.7). With the reduced size of L, the %THD increases to 12.52 %. But with the proposed nominal + ISM based controller the %THD is restricted to 9.26 %.

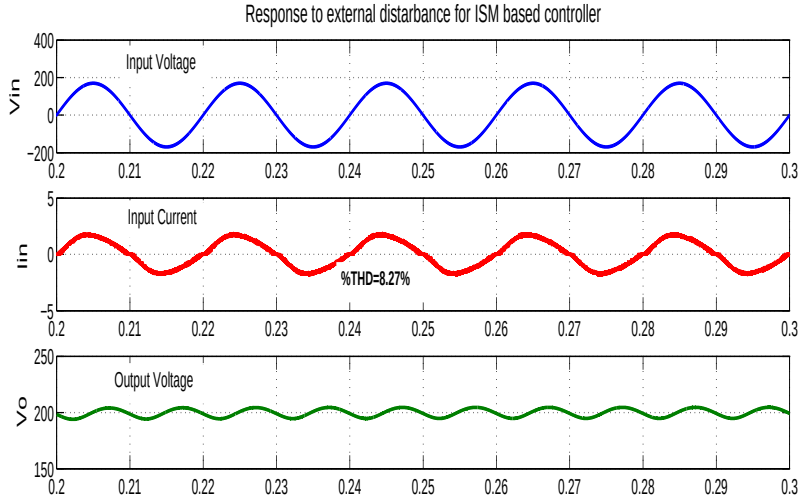

Figure 6.9 : System response using nominal controller +ISMC against the external disturbance.

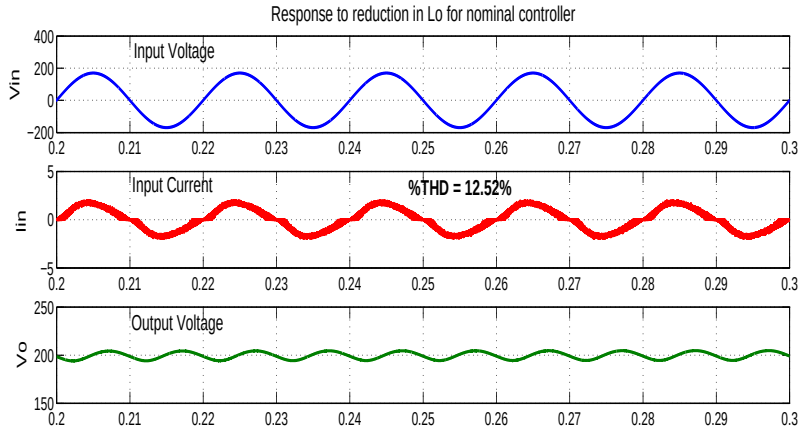

Figure 6.10 : Steady state result for reduced parameters using nominal control.

It is to be noted that the proposed ISM based control, not only minimizes the %THD in input current that is increased due to the reduced size of inductance L with nominal controller alone but also removes the external disturbance caused by 500 Hz disturbance (provided as a 500 Hz frequency sinusoidal function) in the control input. This also concludes that the comparatively smaller size of L and C can be used with ISM based control.

6.3 ISM CONTROLLER FOR Z-SOURCE CONVERTER WITH UNCERTAINTY IN PARAMETERS

In this Section, the effectiveness of the ISM control to compensate for the unmodeled dynamics in a reduced order Z-source is analysed. This work leverages the quality of ISM, of being able to maintain the system performance even under system parameter variation. This section presents the small signal model of the a Z-source converter and then a reduced model for the same is derived. The effect of asymmetry on the system response for the full and reduced models is studied. Later the design of the nominal dual-loop PI control and proposed ISM control is carried

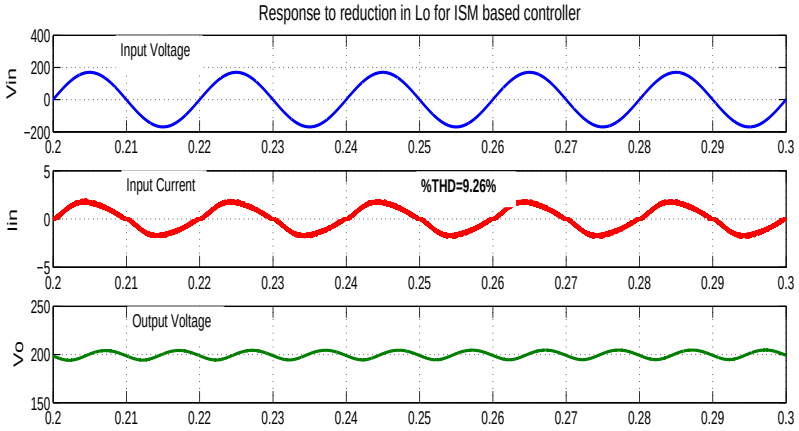

Figure 6.11 : Steady state result for reduced parameters using nominal with ISM based control.

out. Results highlighting the effectiveness of the proposed controller is also demonstrated in the Section.

6.3.1 System description and dynamic modelling

The circuit of the Z-source converter (ZSC), under consideration is shown in Fig. 6.12. In the simplified circuit, the load is in parallel with an active switch S. V_g is an independent voltage source and the load impedance is $Z_l = R_l + sL_l$.

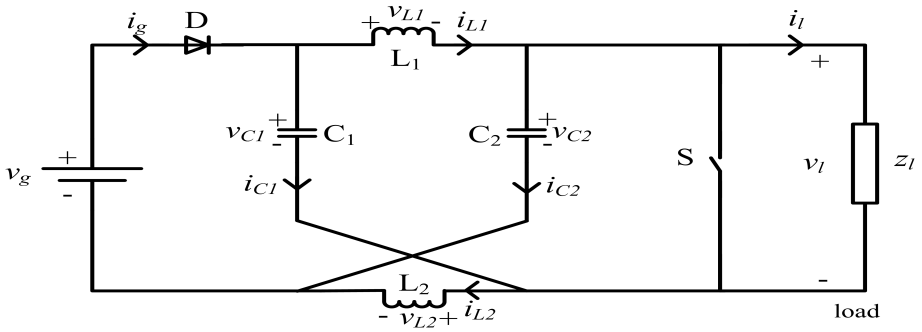

Figure 6.12 : A Z source converter

To design controllers for ZSC, an accurate small signal model of ZSC is needed. Z-source converter is usually modelled as a fifth order system with the two capacitors voltages and two inductor current of the Z-network along with the load current as state variables. The linear model of the converter is obtained using small-signal analysis. This method helps to study the system dynamic response when perturbed by a small disturbance. The variables after perturbation are

$$x = \begin{bmatrix} i_{L1} & i_{L2} & v_{C1} & v_{C2} & i_l \end{bmatrix}$$

d is the perturbed part of the input control signal. I_{L1}, I_{L2}, V_{C1}, V_{C2}, V_g, I_l, D, $D' = (1-D)$ are the nominal operating conditions for the system. The small signal model of the system, obtained using perturbed variables, around the operating point, and collecting only the AC terms, is given as

$$\begin{bmatrix} L_1 & 0 & 0 & 0 & 0 \\ 0 & L_2 & 0 & 0 & 0 \\ 0 & 0 & C_1 & 0 & 0 \\ 0 & 0 & 0 & C_2 & 0 \\ 0 & 0 & 0 & 0 & L_l \end{bmatrix} \begin{bmatrix} \dot{i_{L1}} \\ \dot{i_{L2}} \\ \dot{v_{C1}} \\ \dot{v_{C2}} \\ \dot{i_l} \end{bmatrix} = \begin{bmatrix} 0 & 0 & D & -D' & 0 \\ 0 & 0 & -D' & D & 0 \\ -D & D' & 0 & 0 & -D' \\ D' & -D & 0 & 0 & -D' \\ 0 & 0 & D' & D' & R_l \end{bmatrix} \begin{bmatrix} i_{L1} \\ i_{L2} \\ v_{C1} \\ v_{C2} \\ i_l \end{bmatrix} + \begin{bmatrix} V_{C1}+V_{C2}-V_g \\ V_{C1}+V_{C2}-V_g \\ -I_{L1}-I_{L2}+I_l \\ -I_{L1}-I_{L2}+I_l \\ -V_{C1}-V_{C2}+V_g \end{bmatrix} d \tag{6.36}$$

The DC steady state values satisfy $V_{C1} = V_{C2} = V_C$ and $I_{L1} = I_{L2} = I_L$ because of network symmetry. And the steady state values of the capacitor voltage and the inductor current are

$$\begin{bmatrix} I_L \\ V_C \\ I_l \end{bmatrix} = \begin{bmatrix} I_l \frac{(1-D)}{(1-2D)} \\ V_g \frac{(1-D)}{(1-2D)} \\ \frac{V_C}{R_l} \end{bmatrix}$$

Z-source converters are modelled with five state variables which make them a complex system however, considering the symmetry of the system this full state model is reduced to a three state model considering only one of the inductor current and capacitor voltage along with the load current as state variables. And the new model is given as

$$\begin{bmatrix} L & 0 & 0 \\ 0 & C & 0 \\ 0 & 0 & L_l \end{bmatrix} \begin{bmatrix} \dot{i_L} \\ \dot{v_C} \\ \dot{i_l} \end{bmatrix} = \begin{bmatrix} 0 & 2D-1 & 0 \\ 1-2D & 0 & -(1-D) \\ 0 & 2(1-D) & -R_l \end{bmatrix} \begin{bmatrix} i_L \\ v_C \\ i_l \end{bmatrix} + \begin{bmatrix} 2V_C - V_g \\ -2I_L + I_l \\ -2V_C + V_g \end{bmatrix} d \tag{6.37}$$

The relevant transfer function for the reduced order model is given as:

- The Control input to output voltage transfer function

$$T_{vd}(s) = \frac{v_C(s)}{d(s)}\bigg|_{V_g(s)=0} = \frac{(-2I_L+I_l)L_lLs^2+[(-2I_L+I_l)R_lL+(D'-D)(2V_C-V_g)L_l+LD'(2V_c-V_g)]s+(D'-D)(2V_c-V_g)}{L_lLCs^3+R_lLCs^2+[2D'^2L+L_l(D-D')^2]s+R_l(D-D')^2} \tag{6.38}$$

- The Control input to inductor current transfer function

$$T_{id}(s) = \frac{i_L(s)}{d(s)}\bigg|_{V_g(s)=0} = \frac{(2V_C-V_g)L_lLCs^3+[(2V_C-V_g)R_lLC+(D'-D)(-2I_L+I_l)L_lL]s^2+LD'(2V_c-V_g)+(D'-D)(-2I_L+I_l)R_lLs}{sL[L_lLCs^3+R_lLCs^2+[2D'^2L+L_l(D-D')^2]s+R_l(D-D')^2]} \tag{6.39}$$

- The inductor current to output voltage transfer function

$$T_{vi}(s) = \frac{v_C(s)}{i_L(s)}\bigg|_{V_g(s)=0,d(s)=0} = \frac{sL[(-2I_L+I_l)L_lLs^2+[(-2I_L+I_l)R_lL+(D'-D)(2V_C-V_g)L_l+LD'(2V_c-V_g)]s+(D'-D)(2V_c-V_g)]}{(2V_C-V_g)L_lLCs^3+[(2V_C-V_g)R_lLC+(D'-D)(-2I_L+I_l)L_lL]s^2+LD'(2V_c-V_g)+(D'-D)(-2I_L+I_l)R_lLs} \tag{6.40}$$

Table 6.2 present the system parameters of the undertaken Z source converter. Further analysis will be based on these nominal values.

For the model considered above the pole-zero map of control-to-output-voltage transfer function for a symmetrical full and reduced models is shown in Fig. 6.13 The poles (x) and zeros

Table 6.2 : System Parameters of Z source converter

Parameter	Value
Input Voltage Supply (V_g)	12 V
Reference Output voltage (V_{ref})	20 V
Nominal Duty Cycle D	0.28
Z Inductors ($L_1 = L_2 = L$)	300 μH
Z Capacitors ($C_1 = C_2 = C$)	360 μF
Load Impedance (R_l, L_l)	8.15 Ω,2.1 mH
Switching Frequency f_{sw}	25kHz

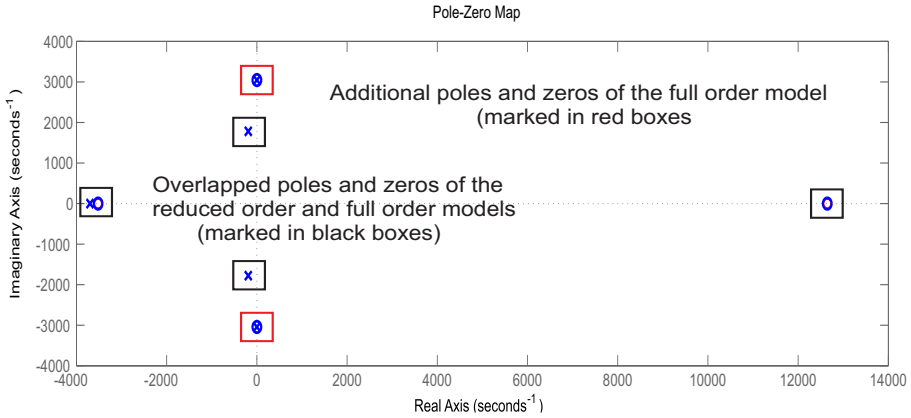

Figure 6.13 : Pole zero map of control-to-capacitor-voltage transfer function for a symmetrical full order and reduced order ZSC

(o) for the two models are presented. The common poles and zeros for the two cases overlapping each other are marked inside black boxes. The additional poles and zeros of the full order model are marked inside red boxes. It shows that for a symmetrical system, the additional poles and zeros of the full order model which are lying on the imaginary axis will cancel each other and hence the system behaviour could be given using reduced model as well.

6.3.2 Proposed ISM Control (The overall control)

The proposed control ($u = u_o + u_n$) for this application, as well, combines a dual-loop PID-control (u_o) and the sliding mode control (u_n). This section proposes the design of the nominal PID control along with the ISM based controller to eliminate the matched uncertainty/disturbances.

6.3.3 Design of PID controller using the Reduced order model

PI controllers are linear control approach which requires a good knowledge of the system and precise tuning in order to obtain the desired performances. For a symmetrical ZSC, a dual loop PI controller was designed using the reduced model given in (6.37). The control structure adopted

is kept as Fig 6.14.

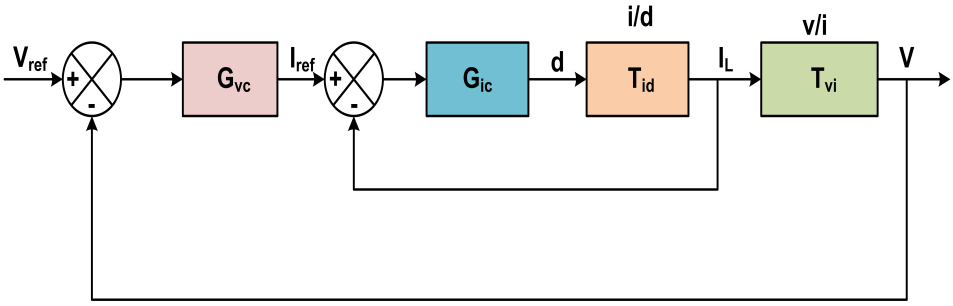

Figure 6.14 : Dual loop control structure

G_{vc} is the controller for outer voltage loop and G_{ic} the controller for inner current loop, T_{id}, T_{vi} are the two linear transfer functions obtained from the linearisation around the equilibrium point.
The control to current output transfer function can be derived from the reduced model as follows

$$T_{id}(s) = \frac{90909(s+3793)(s+527.3)}{(s+3733)(s^2+341.8s+1.957e06)} \tag{6.41}$$

The PI controller is designed as:

$$G_{ic} = \frac{0.17s+0.034}{s} \tag{6.42}$$

The current loop gain can be expressed as

$$G_i = T_{id} * G_{ic} \tag{6.43}$$

The Frequency response curve of the open loop transfer function (T_{id}) and the closed loop gain (G_i) for the inner current loop is plotted in Fig. 6.15, which shows a PM = 89.8 ^{o} at 90.9k rad/s. A PI controller is designed to have a cut-off frequency of $f_{sw}/10$, where, $f_{sw} = 25kHz = 15700rad/s$ and a phase margin of 89.1deg. The designed compensator also increases the low frequency gain and reduce the steady-state error between the desired and actual inductor current.

Now, for the outer loop current to voltage transfer function is obtained as

$$T_{vi} = \frac{-0.16732(s-8518)(s+3495)}{(s+3793)(s+527.3)} \tag{6.44}$$

The PI controller adopted is given as

$$G_{vc} = \frac{1.011s+1011}{s} \tag{6.45}$$

With the inner current loop closed, the outer voltage loop gain can be expressed as a function of inner current loop gain and associated compensator as

$$G_v = T_{vi}\frac{G_i}{(1+G_i)}G_{vc} \tag{6.46}$$

The uncompensated outer loop has a phase margin of 106° at $1.23krad/s$. And the designed controller for this loop must make the compensated system to have a cross-over frequency of about $f_{sw}/100 = 1.52krad/s$. The Voltage-loop frequency domain plot for open-loop transfer function(T_{vi}) and closed-loop gain (G_v) are shown in Fig. 6.16. The phase margin is 66.2°. It also increases the low frequency gain and reduce the steady-state error between the desired and actual inductor current.

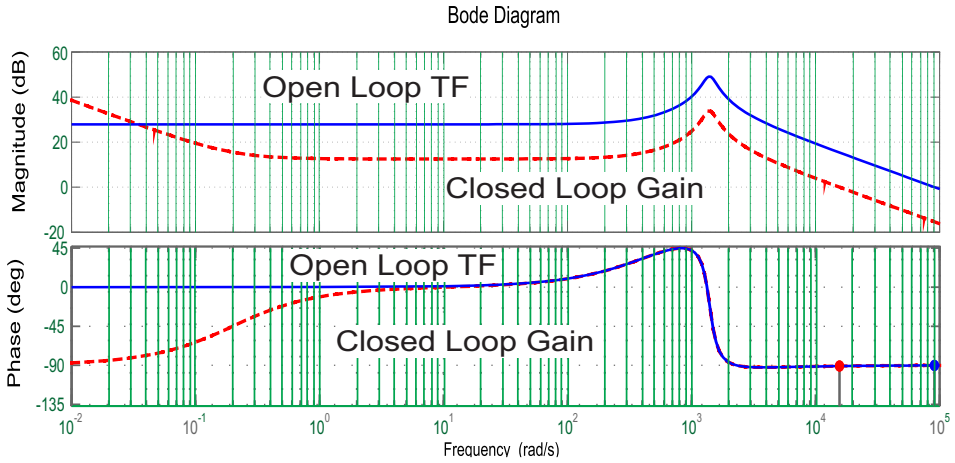

Figure 6.15 : Current-loop frequency domain plot for open-loop transfer function and closed-loop gain: (a) magnitude and (b) phase.

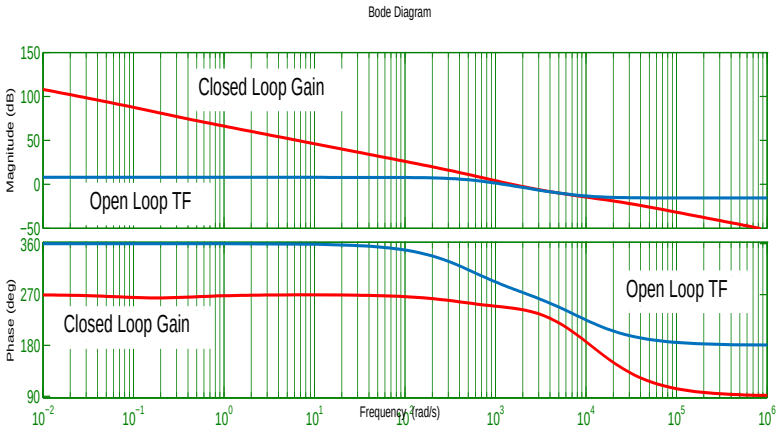

Figure 6.16 : Voltage-loop frequency domain plot for open-loop transfer function and closed-loop gain: (a) magnitude and (b) phase.

Design of ISM based Control

For the reduced model of a Z-source converter, the system dynamics (6.32) can be written as

$$x(t) := \begin{bmatrix} i_L \\ v_C \\ I_l \end{bmatrix}; g_1(x(t)) = \begin{bmatrix} 2V_C - V_g \\ -2I_L + I_l \\ -2V_C + V_g \end{bmatrix};$$

The switching surface is again

$$s(x,t) = G[x(t) - x(0) - \int_0^{\tau} \{f(x(\tau)) + g(x(\tau))u_o(x(\tau))\}d\tau] \tag{6.47}$$

Here, the matrix G is chosen as given in (6.48). $x(0)$ is the initial condition. u_0 is the control input of

nominal PID controller. The total control input (u) is, $u_o + u_n$. For the present Z-source converter

$$G = g^+(x(t)) = \{g^T(x(t))g(x(t))\}^{-1} g^T(x(t)) \tag{6.48}$$

$$g(x(t))^T = \left[\frac{2V_C - V_g}{L} \quad \frac{-2I_L + I_l}{C} \quad \frac{-2V_C + V_g}{L_l}\right];$$

and

$$g^+(x(t)) := \left[\frac{-(V_g - 2V_C)}{L(\frac{(2I_L - I_l)^2}{C^2} + \frac{(V_g - 2*V_C)^2}{L^2} + \frac{(V_g - 2V_C)^2}{L_l^2})} \quad \frac{-(2I_L - I_l)}{C(\frac{(2I_L - I_l)^2}{C^2} + \frac{(V_g - 2V_C)^2}{L^2} + \frac{(V_g - 2V_C)^2}{L_l^2})} \quad \frac{(V_g - 2V_C)}{L_l(\frac{(2I_L - I_l)^2}{C^2} + \frac{(V_g - 2V_C)^2}{L^2} + \frac{(V_g - 2V_C)^2}{L_l^2})}\right]^T$$

This implies $Gg(x(t)) = 1$.

The discontinuous control is kept as

$$u_n = -\eta(Gg(x(t)))^{-1} \frac{s}{||s||} \tag{6.49}$$

The total control is $u = u_o + u_n$. The control is compared against a triangular carrier wave of 25 kHz frequency and generates pulses using pulse width modulation (PWM) method. This pulse train then drives the switch of the Z-source converter.

6.3.4 Effects of Asymmetry in the Z-network

So, far the entire analysis was made on the assumption that the Z-network of the converter is symmetrical, i.e. the two inductors and capacitors are same. However, this assumption of symmetry in the Z-source network is more theoretical than practical. This is because no two elements can be made exactly same and this difference will only grow as the system ages. This section shows how the system poles and zeros change when the network undergoes change from its nominal values. To do so, firstly, the two inductors L_1 and L_2 are made different by changing L_2 to 100 μH. The corresponding pole zero maps for ZSC with asymmetry in inductors L_1 and L_2 are shown in Fig. 6.17

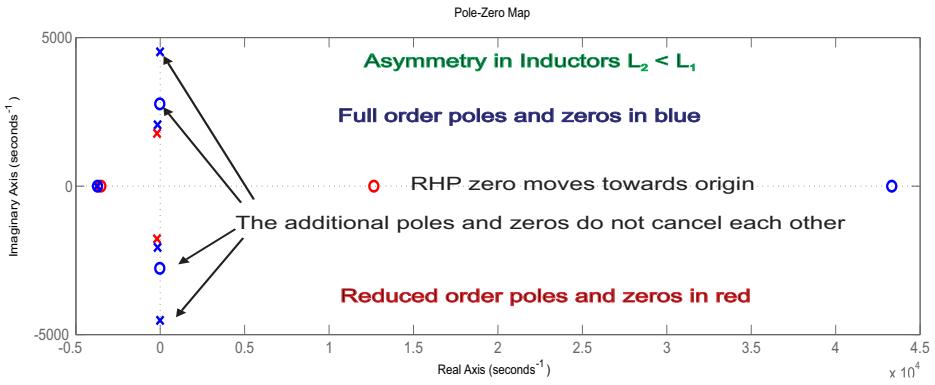

Figure 6.17 : Pole zero map with $L_2 < L_1$ full order and reduced order ZSC

It shows that when L_2 is reduced to 100 μH from the nominal value of 300 μH, the symmetry no longer exists and the pole-zero cancellation at the imaginary axis does not happen. Now, if the difference is due to the change in inductor and capacitor values which are modeled and sensed for the designed controller then it can compensate for the discrepancy. However, if this difference is due to change in unsensed Z-network elements, the controller would not know and hence no compensation is provided.

Therefore, the system dynamics can not be represented by the reduced order model and a controller designed using the reduced order model can no longer suffice. That is where the non-linear ISM controller presents itself as an effective solution. The ISM based controller can compensate for such discrepancy if this parametric uncertainty lies in the matched space of the input.

6.3.5 Simulation Studies

This section presents the simulation study of the proposed control scheme. The results are categorized into three sections; first section demonstrates the effect of asymmetry in system corresponding to the nominal control and proposed ISM based control. In the next section, effectiveness of ISM based controller against external disturbances is explored, and lastly, load transient response for the system is presented.

Effect of system asymmetry

For the analysis purpose, asymmetry is created by changing inductor L_1 from nominal 300 μH to 100 μH. L_2 is kept to its nominal value. The corresponding result in the form of capacitor voltage (V_C) is shown in Fig. 6.18, where, due to symmetry $V_{C1} = V_{C2} = V_C$.

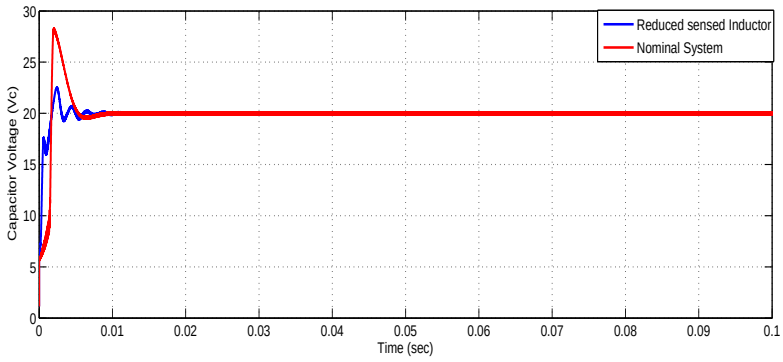

Figure 6.18 : Effect of asymmetry due to reduction in sensed inductor L_1 size

Since the change was made for the modelled inductor, whose current is one of the state variable in the reduced order model, the change is sensed and communicated to the controller. Therefore, as shown, the nominal PI controller can compensate its effects and the capacitor voltage is regulated to its reference value of 20 V.
However, if the discrepancy arises due to the unmodelled inductor dynamics, the system performance degrades as shown in Fig. 6.19. Here, Inductors are made different by changing L_2 to 100 μH while keeping L_1 to its nominal value of 300 μH.

In this case, the dynamics of the inductor L_2 which was changed, was not included in the reduced order model, therefore, the nominal controller was not updated. As a result, the system performance degrades and the capacitor voltage sees high oscillations around the reference voltage of 20 V. On the other hand, ISM based control is effectively able to compensate even this unmodelled system dynamics.

Response to external disturbance

To compare the system response to external disturbances two cases are taken: a) a disturbance introduced in input channel b) a disturbance introduced in generated reference inductor current. The results corresponding to the aforementioned cases are presented here.
The effect of an external disturbance entering through the control input channel is presented in

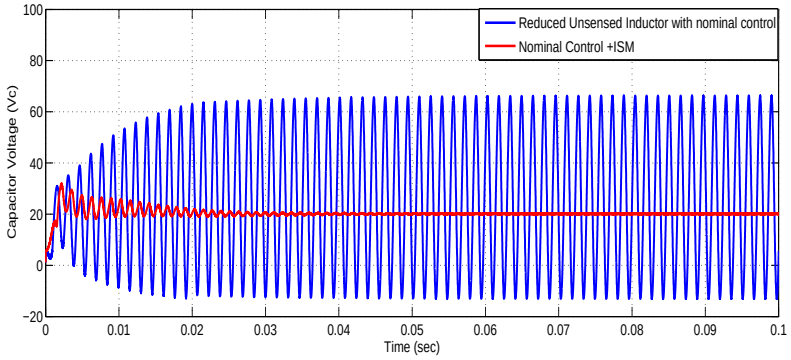

Figure 6.19 : Effect of asymmetry due to reduction in unmodeled inductor L_2 size

Fig. 6.20. An external disturbance $\tilde{d} = 0.2sin(2\pi 500t)$ is added in the input channel. As shown, the nominal controller alone is not able to compensate for this disturbance and the sinusoidal effect gets reflected on the capacitor voltage. The proposed ISM controller, on the other hand, is able to eliminate this matched disturbance and the voltage is regulated to its desired value. The value of η is kept greater than 0.2 that is higher than the amplitude of sinusoidal disturbance, for compensation.

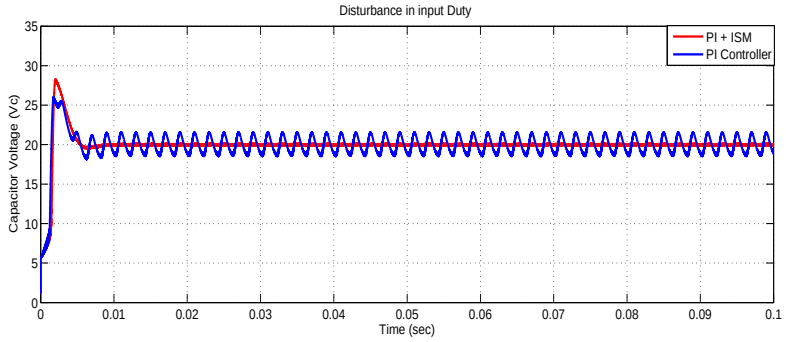

Figure 6.20 : System response to external disturbance in the input channel

Similar to the disturbance in input duty channel, this time an external disturbance $\tilde{d_1} = 0.8sin(2\pi 500t)$ is added in the I_{ref} generated as an output from the outer voltage loop to be fed into the inner current loop. The system response in regulating the inductor current is shown in Fig. 6.21.

The Fig. 6.21 shows that for the nominal controller, the inductor current follows the sinusoidal behaviour imbibed in the reference signal, whereas, the proposed control scheme is able to mitigate this effect. The value of η is kept greater than 0.8 as needed to mitigate disturbance.

Transient response

This section provides the system response to a load variation for the proposed controller. For the analysis, the resistance in the load is changed from 8 Ω to 4 Ω at t = 0.1 sec and result is shown in Fig. 6.22.

As shown in figure, even with the load perturbation, the system maintains it's performance with the proposed controller. The corresponding switching variable s is plotted in Fig. 6.23. It

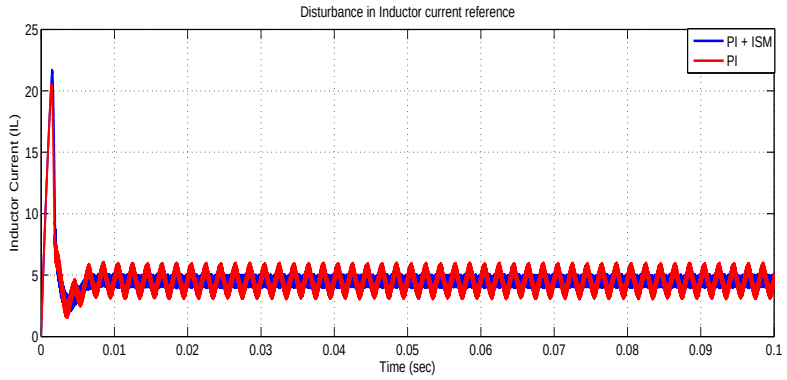

Figure 6.21 : System response to external disturbance in the generated reference current

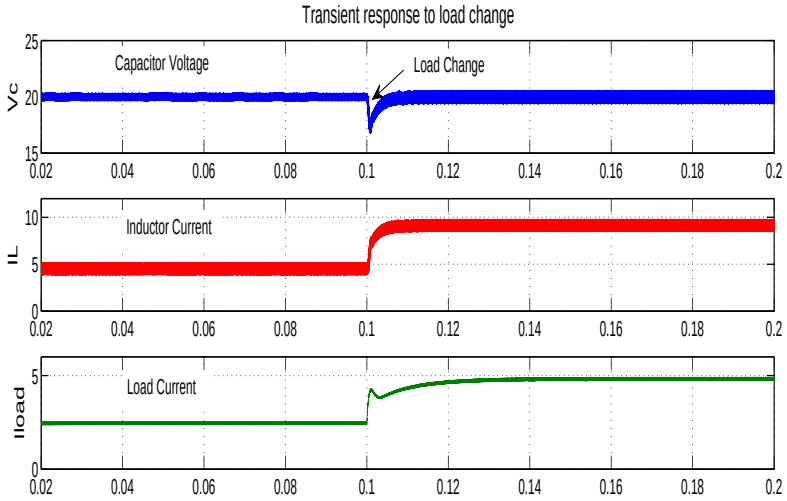

Figure 6.22 : Transient response to load change

stays zero from the initial point, thus eliminating all matched disturbance and providing improved dynamic response to the system.

6.4 SUMMARY

In this Chapter, an ISM based controller has been proposed for a Boost PFC and a Z-source converter application. For Boost PFC, with the nominal PI controller alone, the %THD is 9.6 %. The THD increases to 14.75 % with external disturbance in input channel. However, the harmonics are eliminated and %THD is brought to 8.27 % using proposed ISM based controller. Furthermore, for the parametric variations also ISM was able to compensate for the reduction in inductance unlike nominal PI controller by restricting %THD to 9.26 %. The transient behaviour for the controller was also analysed. In the second section, effect of asymmetry on system response, due to unmodeled dynamics of elements, for a Z-source converter is studied. Proposed control is able to maintain the system performance while when operated with the nominal controller alone, system is effected and provides a highly oscillatory capacitor voltage. Similarly, the effectiveness of the ISM based control against external disturbances and with load variation is established.

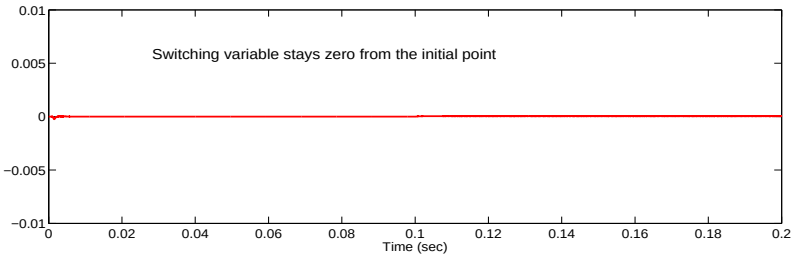

Figure 6.23 : Switchng variable for load variation in ZSC

The following Chapter concludes the Thesis and presents some open challenges yet to be addressed.